Disentangling Transient Charge Density and Metal−Ligand Covalency in Photoexcited Ferricyanide with Femtosecond Resonant Inelastic Soft X-ray Scattering

Raphael M. Jay,[†] Jesper Norell,[‡] Sebastian Eckert,[†,§] Markus Hantschmann,[§] Martin Beye,[§,∥] Brian Kennedy,[§] Wilson Quevedo,[§] William F. Schlotter,[⊥] Georgi L. Dakovski,[⊥] Michael P. Minitti,[⊥] Matthias C. Hoffmann,[⊥] Ankush Mitra,[⊥,●] Stefan P. Moeller,[⊥] Dennis Nordlund,[#] Wenkai Zhang,[#,◆] Huiyang W. Liang,[#] Kristjan Kunnus,[#] Katharina Kubiček,[∥,▲] Simone A. Techert,[∥,@] Marcus Lundberg,[△,▽] Philippe Wernet,[§] Kelly Gaffney,[#] Michael Odelius,[*,‡] and Alexander Föhlisch[*,†,§]

[†]Institut für Physik und Astronomie, Universität Potsdam, 14476 Potsdam, Germany

[‡]Department of Physics, Stockholm University, Albanova University Center, 10691 Stockholm, Sweden

[§]Institute for Methods and Instrumentation for Synchrotron Radiation Research, Helmholtz-Zentrum Berlin für Materialien und Energie GmbH, 12489 Berlin, Germany

[∥]DESY Photon Science, 22607 Hamburg, Germany

[⊥]LCLS, SLAC, Menlo Park, California 94025, United States

[#]PULSE Institute, SLAC, Menlo Park, California 94025, United States

[@]Institute for X-ray Physics, Göttingen University, 37077 Göttingen, Germany

[△]Department of Chemistry - Ångström Laboratory, Uppsala University, 75121 Uppsala, Sweden

[▽]Department of Biotechnology, Chemistry and Pharmacy, Università di Siena, 53100 Siena, Italy

S *Supporting Information*

ABSTRACT: Soft X-ray spectroscopies are ideal probes of the local valence electronic structure of photocatalytically active metal sites. Here, we apply the selectivity of time-resolved resonant inelastic X-ray scattering at the iron L-edge to the transient charge distribution of an optically excited charge-transfer state in aqueous ferricyanide. Through comparison to steady-state spectra and quantum chemical calculations, the coupled effects of valence-shell closing and ligand-hole creation are experimentally and theoretically disentangled and described in terms of orbital occupancy, metal−ligand covalency, and ligand field splitting, thereby extending established steady-state concepts to the excited-state domain. π-Back-donation is found to be mainly determined by the metal site occupation, whereas the ligand hole instead influences σ-donation. Our results demonstrate how ultrafast resonant inelastic X-ray scattering can help characterize local charge distributions around catalytic metal centers in short-lived charge-transfer excited states, as a step toward future rationalization and tailoring of photocatalytic capabilities of transition-metal complexes.
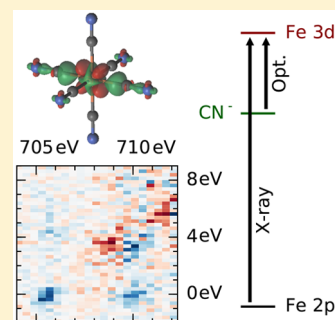
Transition-metal (TM) complexes play a crucial role in photocatalytic processes relevant for a fundamental chemical understanding as well as research on solar fuels.[1] In the latter, catalysts based on the widely abundant and nontoxic iron (Fe) are of particular value.[2] Especially charge-transfer excited states of Fe complexes have attracted considerable scientific interest, as the optically induced redistribution of valence charge density can be exploited in light-harvesting applications.[3] For that purpose, an understanding of how transient charge densities around the metal center govern the ability of TM complexes to facilitate chemical reactions is critical. Specifically, the localization of an electronic charge deficiency or surplus described through orbital occupancy and

metal−ligand covalency has to be characterized and rationalized. Yet, disentangling these properties in real time during photochemical reactions has proven to be spectroscopically challenging.

In recent years, resonant inelastic X-ray scattering (RIXS[4]) at metal L-edges has been established as a powerful probe of the local valence electronic structure in 3d TM compounds.[5−8] With the underlying 2p → 3d core-excitation of the inelastic scattering process, occupied as well as unoccupied valence

orbitals around the central metal are locally accessed, thereby probing both orbital occupancy and metal−ligand covalency. Particularly in conjunction with advanced quantum chemical simulations, the coupled effects of σ-donation and π-back-donation have been disentangled and quantified under steady-state conditions.[6] With the high brilliance and time-resolution of free electron lasers (FELs), the selectivity of RIXS can also be applied to complexes in transient configurations.[9−12] Femtosecond (fs) RIXS at metal L-edges can thus probe the relevant molecular properties to describe transient changes of charge density following an optical excitation and characterize in novel detail the excited-state electronic structure.

In this work, we demonstrate how time-resolved RIXS is able to retrieve previously inaccessible details of a charge-transfer excited state of the prototypical TM complex ferricyanide $[Fe(III)(CN)_6]^{3-}$ in aqueous solution. As prime examples of octahedral back-donating complexes, ferricyanide and its reduced counterpart ferrocyanide $[Fe(II)(CN)_6]^{4-}$ have been targets of various steady-state[6,13−20] and time-resolved[21−25] studies. Here, we investigate the 400 nm ligand-to-metal charge-transfer (LMCT) excitation in ferricyanide.[14] Previous time-resolved studies have used infrared (IR) spectroscopy[21,25] and valence photoemission[24,25] to primarily investigate the relaxation mechanism of the LMCT state, where the ligand-centric character of IR spectroscopy and the restriction of photoemission to occupied orbitals provide an incomplete characterization of the valence electronic structure of the LMCT excited state. In an approximate one-electron picture, the LMCT state can be described as a dipole-allowed excitation that increases the ground state (GS) t_{2g}^5 occupation of ferricyanide (Figure 1a) to t_{2g}^6 (Figure 1b). Locally at the Fe site, the LMCT state therefore exhibits the same formal 3d closed-shell configuration (t_{2g}^6) as ferrocyanide (Figure 1c). In difference to ferrocyanide, however, the excitation also opens a ligand-hole in the t_{1u} manifold of ligand-derived orbitals[14] (Lt_{1u}, see Figure 1b). The in-total six Lt_{1u} orbitals comprise three σ- and three π-derived ligand orbitals that may mix. Thus, the relative σ- and π-character contributions of the ligand-hole and their influence on σ-donation and π-back-donation cannot be predicted a priori. To observe both changes in valence occupancy as well as the implications of the ligand-hole on the transient electronic structure, we therefore compare the Fe L-edge RIXS spectrum of the LMCT state, detected at fs delays of our optical-pump X-ray-probe measurement, to steady-state RIXS spectra of both ferri- and ferrocyanide in their electronic GSs.

The general layout of the experimental station and details of the soft X-ray beamline have been described in previous publications.[26,27] Details on the experimental parameters can be found in the Supporting Information. The time-resolved RIXS data of ferricyanide shown in Figure 1a,b are recorded by scanning the incident X-ray energy and pump−probe delay, while collecting the scattered X-rays. The ferricyanide GS RIXS spectrum in panel a is acquired by integrating over the negative delays up to −70 fs. The main RIXS features in the measured range have previously been assigned and analyzed by Kunnus et al.[6] and Norell et al.[28] Within this study, we therefore focus on spectral features that have been previously identified as fingerprints of the LMCT state[28] and thus are of particular value for its characterization. The corresponding RIXS features of GS ferricyanide are marked in Figure 1a and denoted according to the electronic occupations of frontier orbitals in the RIXS final states. Despite the highly multi-
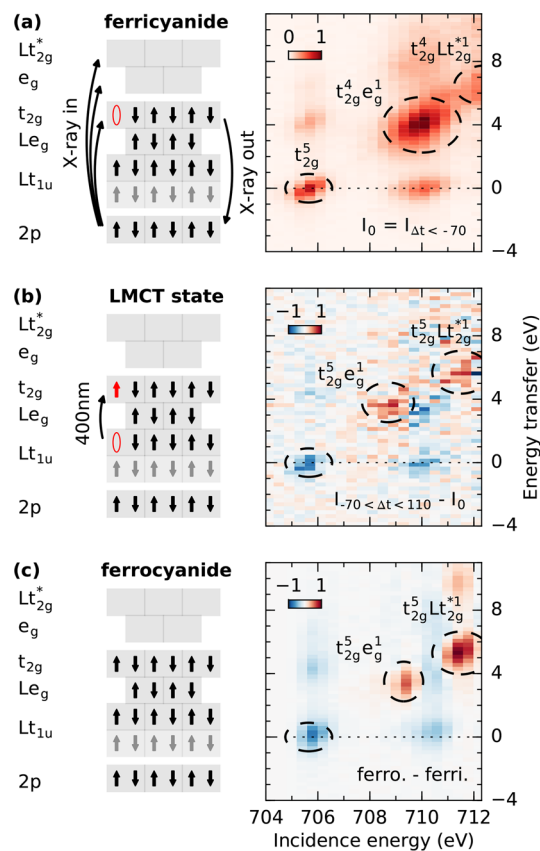

Figure 1. (a) Valence electronic occupation and schematic RIXS process together with the RIXS map of ferricyanide acquired by integrating up to −70 fs delay. Characteristic RIXS features are encircled and denoted according to the assigned final state occupations. (b) Valence electronic occupation of the LMCT state and difference map in the range of −70 to 110 fs. (c) Valence electronic occupation of ferrocyanide and static difference map between ferro- and ferricyanide (data taken from Kunnus et al.[6]), qualitatively reproducing the transients detected in the time-resolved measurements.

configurational nature of the involved states, they can be nominally assigned within a single-electron picture.[6,28] The three features result from core-excitation into the three different (partially) unoccupied valence orbitals (t_{2g}, e_g, and Lt_{2g}^*), with varying energy transfers due to (in)elastic scattering from the t_{2g} orbitals. First, Fe 2p → t_{2g} excitation (705.6 eV incidence energy) causes multiple scattering features indicative of the open-shell t_{2g}^5 configuration of GS ferricyanide, with the elastic peak (0 eV energy transfer) carrying the most intensity. Second, the Fe 2p → e_g excitation (710 eV incidence energy) exhibits significant decay into the $t_{2g}^4 e_g^1$ final state (4 eV energy transfer). Because of its metal-centered dd-character, it is of particular interest as a measure of the ligand field splitting (10Dq) between the t_{2g} and e_g levels.[5] This excitation is dipole-forbidden through direct optical spectroscopy yet uniquely accessible through RIXS. Third, Fe 2p → Lt_{2g}^* excitation (signal beyond 712 eV incidence energy) shows decay into the $t_{2g}^4 Lt_{2g}^{*1}$ final state (7 eV energy transfer). Because of its metal-to-ligand charge-transfer (MLCT) character, it directly probes the relative strength of back-donation into the ligand π*-system.[6]

Following the optical excitation, the early transient spectrum (integrated between −70 and 110 fs) corresponding to the

LMCT state is shown in Figure 1b. Negative delays are included to account for the time-resolution of ~180 fs. The short integration range is chosen to avoid spectral overlap with potential secondary species.[24] The data is displayed as a difference taken with respect to the map in Figure 1a after normalizing to the number of FEL shots included in the respective integrated delay ranges. In terms of final state energies, the LMCT spectrum shows strong similarity to the static difference spectrum between ferro- and ferricyanide shown in Figure 1c. The static difference is generated from the steady-state spectra of Kunnus et al.[6] after normalizing each map to its respective edge-jump (difference of post-edge intensity at 729 eV and below any pre-edge features at 704 eV). The striking similarity between the LMCT state and ferrocyanide has previously been observed with time-resolved photoemission spectroscopy in terms of binding energies of Fe 3d-derived orbitals.[24,25] The ferrocyanide closed-shell config-uration therefore constitutes a good first-order approximation of the valence electronic structure of the LMCT state from an iron-centric perspective. The static difference verifies how the valence-shell-closing of the t_{2g} orbitals in the LMCT state quenches the Fe $2p \rightarrow t_{2g}$ core-excitation, seen as a bleach of the ferricyanide t_{2g}^5 final state in the transient map of the LMCT state (Figure 1b) and previously predicted as a spectroscopic fingerprint of the LMCT state.[28] By comparison to ferrocyanide[6] or computational predictions of the LMCT spectrum,[28] the remaining marked transient RIXS features of the LMCT state can now be assigned to $t_{2g}^5 e_g^1$ dd character (709 eV incidence energy, 4 eV energy transfer) and $t_{2g}^5 Lt_{2g}^{*1}$ MLCT character (711.5 eV incidence energy, 5 eV energy transfer).

Despite the similarities between the LMCT state and ferrocyanide, differences in terms of width and position of the $t_{2g}^5 e_g^1$ final state can be observed, which can be assumed to result from the ligand-hole. Figure 2a shows the partial
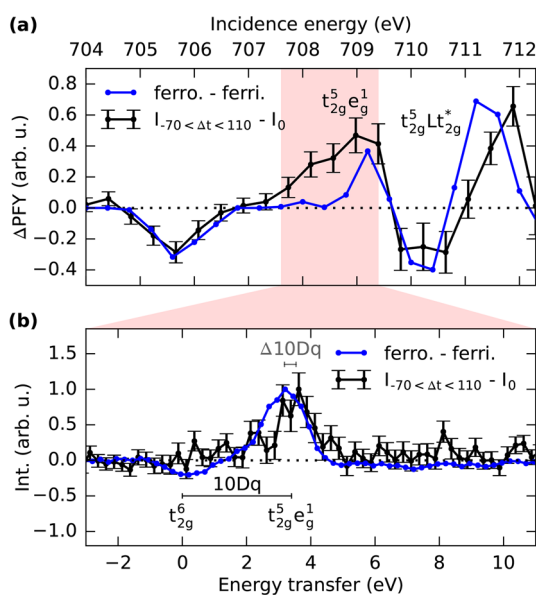
fluorescence yield (PFY) X-ray absorption spectra of the LMCT state and ferrocyanide, taken as differences with respect to ferricyanide. The PFY spectra are generated from the RIXS difference maps (Figure 1b,c) by integration over energy transfers in the range of 2–7.5 eV, thereby isolating the $t_{2g}^5 e_g^1$ and $t_{2g}^5 Lt_{2g}^{*1}$ final states discussed above. To enable a qualitative comparison, the PFY difference intensities are normalized to the respective depletion of the ferricyanide t_{2g}^5 final state (integrated in the range of 704.9–706.7 eV incidence energy, −1.2–1.2 eV energy transfer). In the difference PFY of the LMCT state, the onset of the $t_{2g}^5 e_g^1$ final state is at lower incident energy than in ferrocyanide. Such a shift can be interpreted to reflect stabilizing interactions between an increased electron density at the metal site and the core-hole, leading to smaller core-excitation energies. This can result from varying metal–ligand covalency, which has previously been observed when comparing Fe complexes with different ligands.[29] Of particular interest here is therefore the $t_{2g}^5 Lt_{2g}^{*1}$ final state intensity in Figure 2a, as it directly probes the strength of π-back-donation. The feature exhibits similar intensity in the LMCT state and ferrocyanide, which indicates comparable back-donation of Fe 3d electron density to the Lt_{2g}^* orbitals for the two species. This is consistent with previous studies, where the t_{2g} occupation (same for LMCT state and ferrocyanide) was found to mainly govern π-back-donation.[6] With comparable π-back-donation in both species, the overall increase of charge density at the Fe site in the LMCT state relative to ferrocyanide (as deduced from the shift of the PFY onset) can therefore be expected to result from increased σ-donation, caused by the ligand-hole in the LMCT state. Enhanced electron donation with constant back-donation would strengthen the overall bond between metal and ligand, likely to be reflected in 10Dq. Figure 2b shows the intensity of the $t_{2g}^5 e_g^1$ final state integrated in the incidence energy range of 707.6–709.4 eV and displayed as a function of the energy transfer. The peak positions of the $t_{2g}^5 e_g^1$ final state on the energy-transfer axis are fitted with Gaussian functions and indeed indicate a rougly 10% increase of 10Dq ($\Delta E = (0.3 \pm 0.1)$ eV) in the LMCT state as compared to ferrocyanide. We emphasize that these trends in both excited-state covalencies and ligand field parameters are directly inferred from time-resolved L-edge RIXS, making it a powerful probe of transient charge distributions of photoexcited metal sites.

To corroborate the interpretations of the observed spectral trends and further characterize the electronic structure of the LMCT state, calculations at the complete active space level (CASSCF)[30] with second-order perturbation theory (CASPT2)[31] were carried out for ferricyanide, its LMCT state, and ferrocyanide with the Molcas 8.0 program.[32] Details on the calculations can be found in the Supporting Information. While our previously published restricted active space simulations[6,28] reproduce the overall RIXS spectral trends of all species, positions and intensities of features which involve Fe $2p \rightarrow Lt_{2g}^*$ excitation have been found to depend particularly strongly on the computational parameters.[33] For the most accurate state characterization we therefore resort to single-state calculations that include 13 of the valence orbitals illustrated in Figure 1 in an unbiased complete active space. Because of the severe computational cost scaling of such calculations it is not possible to simultaneously include all six of the Lt_{1u} orbitals as an addition to our previously established[28,33] valence active space of 10 gerade orbitals. While only three of the Lt_{1u} orbitals are thus directly included

Figure 2. (a) Difference PFYs of the LMCT state and ferrocyanide with respect to ferricyanide generated by integration of the RIXS maps in Figure 1b,c over energy transfers in the range of 2–7.5 eV. (b) Difference emission spectra of the LMCT state and ferrocyanide with respect to ferricyanide at the e_g resonance (integrated from 707.6 to 709.4 eV and normalized to the maximum intensity).

in the active space, they are allowed to mix with the remaining three through the self-consistent orbital optimization, and all six are correlated through the subsequent multiconfigurational perturbation theory.

To visualize the results of the calculations in a many-electron description, we turn to the charge density difference (CDD) plots displayed in Figure 3a. The orbitals representing the hole
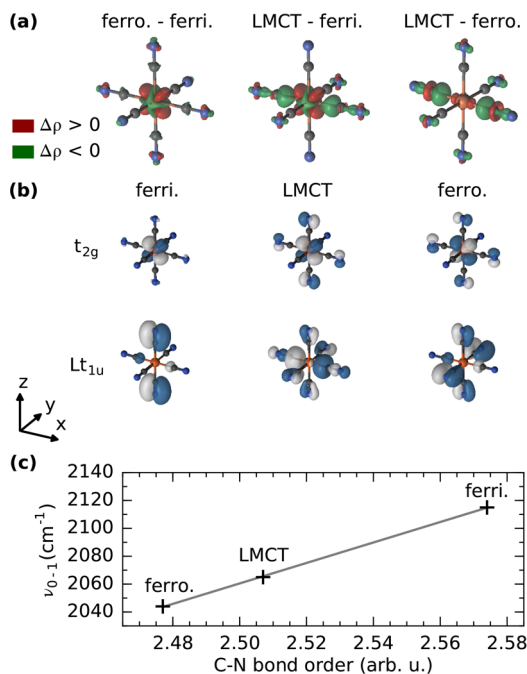

Figure 3. (a) Charge density differences (CDDs) of the LMCT state and ferrocyanide taken with respect to ferricyanide. To isolate ligand-hole effects, the CDD of the LMCT state with respect to ferrocyanide is additionally shown. All differences are calculated at the CASPT2 level within the optimized geometry of ferricyanide. (b) Orbitals containing the hole are shown for ferricyanide and the LMCT state. The corresponding active (fully filled) orbitals of ferrocyanide are displayed in addition. (c) Literature values of the CN-stretch frequencies[13,25] as a function of the calculated average C−N bond order.

in ferricyanide (t_{2g}) and the LMCT state (Lt_{1u}) are displayed in Figure 3b along with the corresponding (fully filled) orbitals of ferrocyanide. The CDDs are calculated for the optimized structure of ferricyanide, which exhibits a small Jahn−Teller distortion due to the open t_{2g}-shell[24,28] that leads to the symmetry-reduced (D_{4h}) behavior of the individual orbitals. The CDDs clearly confirm the local similarities between ferrocyanide and the LMCT state as experimentally observed from Fe L-edge RIXS. With ferricyanide as a reference (Figure 3a, left and middle), ferrocyanide and the LMCT state both exhibit a distinct increase in charge at the metal center in a shape that resembles the t_{2g} orbital, hence directly resulting from its increased occupation (Figure 3b). Both species additionally exhibit a decrease in charge even closer to the metal center, which in an indirect manner also results from the increased t_{2g} occupation. The reduced electron repulsion between metal 3d and ligand electron density in ferricyanide allows for stronger electron donation than in ferrocyanide.[6,15] The same appears to hold in the LMCT state. A quantification of the metal−ligand covalencies is found in Table 1, where the Fe 3d contents of the Le_g and Lt_{2g}^* orbitals are presented as

Table 1. Metal−Ligand Covalency as Expressed through the Summed Fe 3d Atomic Orbital Contents of the σ-Donating Le_g and π-Accepting Lt_{2g}^* Molecular Orbitals[a]

	ferricyanide	LMCT state	ferrocyanide
Le_g	22.4	15.9	14.1
	24.8	19.4	14.7
mean	23.6	17.7	14.4
Lt_{2g}^*	3.8	10.7	10.6
	5.9	11.1	11.0
	5.9	10.7	11.0
mean	5.2	10.8	10.9

[a]The values are presented as percentages normalized to the total contributions of all atomic orbitals to the respective molecular orbital.

they are generally used to measure the strength of σ-donation and π-back-donation, respectively. The orbital contents confirm the general trend of reduced σ-donation and increased π-back-donation as a result of increased t_{2g} occupation in both ferrocyanide and the LMCT state.

Similar to the experimental findings, the differences regarding the electronic structure of the LMCT state and ferrocyanide as compared to ferricyanide therefore appear to be mainly determined by the t_{2g} occupation. Still, smaller differences can also be observed as an effect of the reduced electron density at the ligands in the LMCT state. This can be seen in the CDD of the LMCT state with respect to ferrocyanide (Figure 3a, right), where a charge decrease is present on the ligand x-axis, which can be interpreted as the ligand-hole created by the optical excitation. In accordance with previous denotation,[6,28] the ferricyanide and ferrocyanide Lt_{1u} orbitals included in the active space (i.e., the three out of six most correlated) are of predominantly π character (Figure 3b, left and right). However, the excitation in the LMCT state appears to be from a σ-dominated Lt_{1u} orbital (Figure 3b, middle). Consequently, upon optical excitation, the electron−hole appears to be localized to the σ- rather than to the π-system, as a result of orbital relaxation within the Lt_{1u} manifold.

The creation of a hole in a Lt_{1u} orbital, which is of strong σ-character and essentially nonbonding with respect to the Fe−C bond, decreases electron density between the Fe site and the ligand (Figure 3a, right) while not significantly affecting the bond. It instead allows for better overlap between Fe 3d and Le_g orbitals. The improved overlap counteracts the effect of lowering the ligand orbital energies, which should make the ligand a poorer σ-donor.[34] The result is a net increase in σ-donation with respect to ferrocyanide (compare Table 1) and thus higher electron density on the metal, which is indeed visible on the CDD between the LMCT state and ferrocyanide (Figure 3a, right). This picture is also consistent with the reduced Fe−C bond length in the LMCT state compared to ferrocyanide seen in previous calculations.[6,28] With constant π-back-donation, this indicates an overall stronger bonding interaction between metal and the ligands in the LMCT state than in ferrocyanide. We emphasize that this fully confirms the experimental observations of the PFY onset shift to lower energies as well as an increase of 10Dq in the LMCT state.

Notably, our results are also fully compatible with previous interpretations of steady-state and time-resolved IR-spectroscopy. Shifts of the intraligand IR-stretch frequencies have been shown to typically accompany changes in covalency. This correlation has been established by steady-state IR and

confirmed by X-ray absorption and RIXS measurements upon comparison of metal cyanides in different oxidation states.[6,13,15] Figure 3c shows literature values of the IR-stretch frequencies of ferricyanide, the LMCT state, and ferrocyanide[13,25] as a function of the C−N bond order obtained from our CASPT2 calculations. The bond orders averaged over all ligands scale linearly with the IR-stretch frequencies, thereby accurately reproducing the continuous blue-shift in the order ferrocyanide, LMCT state, and ferricyanide. This agreement therefore confirms the accuracy with which our electronic structure calculations describe the bonding within all three species. While the IR blue-shift of ferricyanide with respect to both other species is then well-explained by the smaller π-back-donation into the C−N antibonding Lt_{2g}^* orbitals, the difference between ferrocyanide and the LMCT state must, because of their similar π-back-donation, instead result from the ligand-hole. However, it is difficult to break down and attribute the difference to changes in single orbitals with respect to their character and occupation. Further rationalization of the C−N bonding is therefore better left for studies with a ligand- rather than metal-centric probe.

In summary, the current work demonstrates that fs RIXS can be applied to derive a detailed metal-centric characterization of transient charge distributions in photoexcited TM complexes in terms of orbital occupation and metal−ligand covalency. Specifically, by studying the LMCT state of ferricyanide we find that π-back-donation is primarily determined by the metal site occupation, whereas σ-donation is influenced by the presence of the ligand-hole, a conclusion that underscores the value of steady-state concepts for interpreting the properties of electronic-excited states. The two effects are experimentally disentangled by comparison to steady-state measurements of ferrocyanide but are also fully corroborated by comparison to quantum chemical calculations. We therefore believe that the access to the transient charge distribution provided by time-resolved L-edge RIXS will be generally applicable to a wide range of chemical reactions involving TM complexes. As electronic charge and its deficiency are drivers of chemical reactivity, detailed insight into the transient electronic structure of the catalytic center can aid in understanding and tailoring chemical properties of photoactivated TM complexes.

ASSOCIATED CONTENT

Ⓢ Supporting Information

The Supporting Information is available free of charge on the ACS Publications website at DOI: 10.1021/acs.jpclett.8b01429.

Experimental and computational details (PDF)

AUTHOR INFORMATION

Corresponding Authors
*E-mail: odelius@fysik.su.se.
*E-mail: alexander.foehlisch@helmholtz-berlin.de.
ORCID
Raphael M. Jay: 0000-0001-9607-8264
Jesper Norell: 0000-0003-1058-2588
Martin Beye: 0000-0002-3924-2993
Huiyang W. Liang: 0000-0001-6548-2061
Marcus Lundberg: 0000-0002-1312-1202
Philippe Wernet: 0000-0001-7011-9072
Michael Odelius: 0000-0002-7023-2486

Present Addresses
◉A.M.: Elementary Particle Physics Group, Department of Physics, University of Warwick, Coventry CV4 7AL, United Kingdom.
◆W.Z.: Center for Advanced Quantum Studies, Department of Physics, Beijing Normal University, Beijing 100875, China.
▲K. Kubiček: European XFEL, 22869 Schenefeld, Germany.

Notes
The authors declare no competing financial interest.

REFERENCES

(1) Gray, H. B.; Maverick, A. W. Solar Chemistry of Metal Complexes. *Science* **1981**, *214*, 1201−1205.
(2) Chirik, P. J. Iron- and Cobalt-Catalyzed Alkene Hydrogenation: Catalysis with Both Redox-Active and Strong Field Ligands. *Acc. Chem. Res.* **2015**, *48*, 1687−1695.
(3) Liu, Y.; Persson, P.; Sundström, V.; Wärnmark, K. Fe N-Heterocyclic Carbene Complexes as Promising Photosensitizers. *Acc. Chem. Res.* **2016**, *49*, 1477−1485.
(4) Ament, L. J. P.; van Veenendaal, M.; Devereaux, T. P.; Hill, J. P.; van den Brink, J. Resonant Inelastic X-ray Scattering Studies of Elementary Excitations. *Rev. Mod. Phys.* **2011**, *83*, 705−767.
(5) van Schooneveld, M. M.; Gosselink, R. W.; Eggenhuisen, T. M.; Al Samarai, M.; Monney, C.; Zhou, K. J.; Schmitt, T.; de Groot, F. M. F. A Multispectroscopic Study of 3 d Orbitals in Cobalt Carboxylates:

The High Sensitivity of 2p3d Resonant X-ray Emission Spectroscopy to the Ligand Field. *Angew. Chem., Int. Ed.* **2013**, *52*, 1170−1174.

(6) Kunnus, K.; Zhang, W.; Delcey, M. G.; Pinjari, R. V.; Miedema, P. S.; Schreck, S.; Quevedo, W.; Schröder, H.; Föhlisch, A.; Gaffney, K. J.; et al. Viewing the Valence Electronic Structure of Ferric and Ferrous Hexacyanide in Solution from the Fe and Cyanide Perspectives. *J. Phys. Chem. B* **2016**, *120*, 7182−7194.

(7) Liu, B.; Wang, R.-P.; Glass, E. N.; Hill, C. L.; Cuk, T.; Okamoto, J.; Huang, D.-J.; van Schooneveld, M. M.; de Groot, F. M. F. Distorted Tetrahedral Co II in K 5 H[CoW 12 O 40]· x H 2 O Probed by 2p3d Resonant Inelastic X-ray Scattering. *Inorg. Chem.* **2016**, *55*, 10152−10160.

(8) Hahn, A. W.; Van Kuiken, B. E.; Al Samarai, M.; Atanasov, M.; Weyhermüller, T.; Cui, Y. T.; Miyawaki, J.; Harada, Y.; Nicolaou, A.; DeBeer, S. Measurement of the Ligand Field Spectra of Ferrous and Ferric Iron Chlorides Using 2p3d RIXS. *Inorg. Chem.* **2017**, *56*, 8203−8211.

(9) Wernet, P.; Kunnus, K.; Josefsson, I.; Rajkovic, I.; Quevedo, W.; Beye, M.; Schreck, S.; Grübel, S.; Scholz, M.; Nordlund, D.; et al. Orbital-Specific Mapping of the Ligand Exchange Dynamics of Fe(CO)5 in Solution. *Nature* **2015**, *520*, 78−81.

(10) Kunnus, K.; Josefsson, I.; Rajkovic, I.; Schreck, S.; Quevedo, W.; Beye, M.; Weniger, C.; Grübel, S.; Scholz, M.; Nordlund, D.; et al. Identification of the Dominant Photochemical Pathways and Mechanistic Insights to the Ultrafast Ligand Exchange of Fe(CO) 5 to Fe(CO) 4 EtOH. *Struct. Dyn.* **2016**, *3*, 043204.

(11) Kunnus, K.; Josefsson, I.; Rajkovic, I.; Schreck, S.; Quevedo, W.; Beye, M.; Grübel, S.; Scholz, M.; Nordlund, D.; Zhang, W.; et al. Anti-Stokes Resonant X-ray Raman Scattering for Atom Specific and Excited State Selective Dynamics. *New J. Phys.* **2016**, *18*, 103011.

(12) Eckert, S.; Norell, J.; Miedema, P. S.; Beye, M.; Fondell, M.; Quevedo, W.; Kennedy, B.; Hantschmann, M.; Pietzsch, A.; Van Kuiken, B. E.; et al. Ultrafast Independent N-H and N-C Bond Deformation Investigated with Resonant Inelastic X-Ray Scattering. *Angew. Chem., Int. Ed.* **2017**, *56*, 6088−6092.

(13) Jones, L. H. Nature of Bonding in Metal Cyanide Complexes as Related to Intensity and Frequency of Infrared Absorption Spectra. *Inorg. Chem.* **1963**, *2*, 777−780.

(14) Alexander, J. J.; Gray, H. B. Electronic Structures of Hexacyanometalate Complexes. *J. Am. Chem. Soc.* **1968**, *90*, 4260−4271.

(15) Hocking, R. K.; Wasinger, E. C.; de Groot, F. M. F.; Hodgson, K. O.; Hedman, B.; Solomon, E. I. Fe L-Edge XAS Studies of K 4 [Fe(CN) 6] and K 3 [Fe(CN) 6]: A Direct Probe of Back-Bonding. *J. Am. Chem. Soc.* **2006**, *128*, 10442−10451.

(16) Seidel, R.; Thürmer, S.; Moens, J.; Geerlings, P.; Blumberger, J.; Winter, B. Valence Photoemission Spectra of Aqueous Fe2+/3+ and [Fe(CN)6]4-/3- and their Interpretation by DFT Calculations. *J. Phys. Chem. B* **2011**, *115*, 11671−11677.

(17) Lundberg, M.; Kroll, T.; Debeer, S.; Bergmann, U.; Wilson, S. A.; Glatzel, P.; Nordlund, D.; Hedman, B.; Hodgson, K. O.; Solomon, E. I. Metal-Ligand Covalency of Iron Complexes from High-Resolution Resonant Inelastic X-ray Scattering. *J. Am. Chem. Soc.* **2013**, *135*, 17121−17134.

(18) Penfold, T. J.; Reinhard, M.; Rittmann-Frank, M. H.; Tavernelli, I.; Rothlisberger, U.; Milne, C. J.; Glatzel, P.; Chergui, M. X-ray Spectroscopic Study of Solvent Effects on the Ferrous and Ferric Hexacyanide Anions. *J. Phys. Chem. A* **2014**, *118*, 9411−9418.

(19) Prampolini, G.; Yu, P.; Pizzanelli, S.; Cacelli, I.; Yang, F.; Zhao, J.; Wang, J. Structure and Dynamics of Ferrocyanide and Ferricyanide Anions in Water and Heavy Water: An Insight by MD Simulations and 2D IR spectroscopy. *J. Phys. Chem. B* **2014**, *118*, 14899−14912.

(20) Ross, M.; Andersen, A.; Fox, Z. W.; Zhang, Y.; Hong, K.; Lee, J.-H.; Cordones, A.; March, A. M.; Doumy, G.; Southworth, S. H.; et al. Comprehensive Experimental and Computational Spectroscopic Study of Hexacyanoferrate Complexes in Water: From Infrared to X-ray Wavelengths. *J. Phys. Chem. B* **2018**, *122*, 5075−5086.

(21) Zhang, W.; Ji, M.; Sun, Z.; Gaffney, K. J. Dynamics of Solvent-Mediated Electron Localization in Electronically Excited Hexacyanoferrate(III). *J. Am. Chem. Soc.* **2012**, *134*, 2581−2588.

(22) Reinhard, M.; Penfold, T. J.; Lima, F. A.; Rittmann, J.; Rittmann-Frank, M. H.; Abela, R.; Tavernelli, I.; Rothlisberger, U.; Milne, C. J.; Chergui, M. Photooxidation and Photoaquation of Iron Hexacyanide in Aqueous Solution: A Picosecond X-ray Absorption Study. *Struct. Dyn.* **2014**, *1*, 024901.

(23) Reinhard, M.; Auböck, G.; Besley, N. A.; Clark, I. P.; Greetham, G. M.; Hanson-Heine, M. W. D.; Horvath, R.; Murphy, T. S.; Penfold, T. J.; Towrie, M.; et al. Photoaquation Mechanism of Hexacyanoferrate(II) Ions: Ultrafast 2D UV and Transient Visible and IR Spectroscopies. *J. Am. Chem. Soc.* **2017**, *139*, 7335−7347.

(24) Engel, N.; Bokarev, S. I.; Moguilevski, A.; Raheem, A.; Al-Obaidi, R.; Möhle, T.; Grell, G.; Siefermann, K. R.; Abel, B.; Aziz, S.; et al. Light-Induced Relaxation Dynamics in the Ferricyanide Ion Revisited with Ultrafast XUV Photoelectron Spectroscopy. *Phys. Chem. Chem. Phys.* **2017**, *19*, 14248.

(25) Ojeda, J.; Arrell, C. A.; Longetti, L.; Chergui, M.; Helbing, J. Charge-Transfer and Impulsive Electronic-to-Vibrational Energy Conversion in Ferricyanide: Ultrafast Photoelectron and Transient Infrared Studies. *Phys. Chem. Chem. Phys.* **2017**, *19*, 17052−17062.

(26) Kunnus, K.; Rajkovic, I.; Schreck, S.; Quevedo, W.; Eckert, S.; Beye, M.; Suljoti, E.; Weniger, C.; Kalus, C.; Grübel, S.; et al. A Setup for Resonant Inelastic Soft X-ray Scattering on Liquids at Free Electron Laser Light Sources. *Rev. Sci. Instrum.* **2012**, *83*, 123109.

(27) Schlotter, W. F.; Turner, J. J.; Rowen, M.; Heimann, P.; Holmes, M.; Krupin, O.; Messerschmidt, M.; Moeller, S.; Krzywinski, J.; Soufli, R.; et al. The Soft X-ray Instrument for Materials Studies at the Linac Coherent Light Source X-ray Free-Electron Laser. *Rev. Sci. Instrum.* **2012**, *83*, 043107.

(28) Norell, J.; Jay, R. M.; Hantschmann, M.; Eckert, S.; Guo, M.; Gaffney, K. J.; Wernet, P.; Lundberg, M.; Föhlisch, A.; Odelius, M. Fingerprints of Electronic, Spin and Structural Dynamics from Resonant Inelastic Soft X-ray Scattering in Transient Photo-Chemical Species. *Phys. Chem. Chem. Phys.* **2018**, *20*, 7243−7253.

(29) Godehusen, K.; Richter, T.; Zimmermann, P.; Wernet, P. Iron L-Edge Absorption Spectroscopy of Iron Pentacarbonyl and Ferrocene in the Gas Phase. *J. Phys. Chem. A* **2017**, *121*, 66−72.

(30) Roos, B. O.; Taylor, P. R.; Sigbahn, P. E. A Complete Active Space SCF Method (CASSCF) Using a Density Matrix Formulated Super-CI Approach. *Chem. Phys.* **1980**, *48*, 157−173.

(31) Andersson, K.; Malmqvist, P.-Å.; Roos, B. O. Second-Order Perturbation Theory with a Complete Active Space Self-Consistent Field Reference Function. *J. Chem. Phys.* **1992**, *96*, 1218−1226.

(32) Aquilante, F.; Autschbach, J.; Carlson, R. K.; Chibotaru, L. F.; Delcey, M. G.; De Vico, L.; Fdez. Galván, I.; Ferré, N.; Frutos, L. M.; Gagliardi, L.; et al. Molcas 8: New Capabilities for Multiconfigurational Quantum Chemical Calculations Across the Periodic Table. *J. Comput. Chem.* **2016**, *37*, 506−541.

(33) Pinjari, R. V.; Delcey, M. G.; Guo, M.; Odelius, M.; Lundberg, M. Restricted Active Space Calculations of L-edge X-ray Absorption Spectra: From Molecular Orbitals to Multiplet States. *J. Chem. Phys.* **2014**, *141*, 124116.

(34) Shriver, D. F.; Posner, J. Bridge Addition Compounds. III. The Influence of Boron-Containing Lewis Acids on Electronic Spectra, Vibrational Spectra, and Oxidation Potentials of Some Iron-Cynanide Complexes. *J. Am. Chem. Soc.* **1966**, *88*, 1672−1677.